ARTICLE

Microstructures and Thermophysical Properties of Cu-Fe$_{64}$Ni$_{32}$Co$_4$ Alloys

Wang Cuiping[1],   Le Fancheng[1],   Zhu Jiahua[1],   Yang Mujin[1],   Yang Shuiyuan[1],

Zhang Jinbin[1],   K. Ishida[3],   Liu Xingjun[1, 2]

[1] Fujian Provincial Key Laboratory of Materials Genome, Xiamen University, Xiamen 361005, China; [2] Harbin Institute of Technology, Shenzhen 518055, China; [3] Graduate School of Engineering, Tohoku University, Sendai, 980-8579, Japan

Abstract: Based on the calculation of phase diagrams (CALPHAD) approach and vacuum arc melting technology, the Cu$_x$(Fe$_{0.64}$Ni$_{0.32}$Co$_{0.04}$)$_{100-x}$(x=30, 45, 60, wt%) series alloys were designed and prepared. The effects of annealing process on microstructures, thermal conductivity (TC) and coefficient of thermal expansion (CTE) were investigated for these prepared alloys. The result shows that the Cu-Fe$_{64}$Ni$_{32}$Co$_4$ isotropic polycrystalline alloys present two separate fcc phases (fcc Cu-rich phase and fcc (Fe, Ni, Co)-rich phase) microstructures after annealing at 600 and 800 °C. After annealing at 600 °C for 50 h, the CTE of the alloys ranges from 6.88×10^{-6} to 12.36×10^{-6} K^{-1} and TC varies from 22.91 to 56.13 W·(m·K)$^{-1}$. The TC are significantly higher than that of Invar alloy, and the CTE of Cu$_{30}$(Fe$_{0.64}$Ni$_{0.32}$Co$_{0.04}$)$_{70}$ and Cu$_{45}$(Fe$_{0.64}$Ni$_{0.32}$Co$_{0.04}$)$_{55}$ alloys can well match with that of semiconductor in electronic packaging.

Key words: calculation of phase diagrams approach; Cu-Fe$_{64}$Ni$_{32}$Co$_4$ alloy; microstructures; thermal conductivity; thermal expansion coefficients

With the rapid development towards high-integration and miniaturization in electronics industry, there is an increasing requirement of electronic packaging materials with high performance[1-3]. Electronic packaging materials are widely used in electronic devices to protect and support integrated circuits and other components[4]. There are several principles for these packaging materials as follows: Firstly, these materials should have high thermal conductivity (TC) to deliver the heat. Secondly, they should own a low coefficient of thermal expansion (CTE) about $4 \times 10^{-6} \sim 8 \times 10^{-6}$ K^{-1}[1, 5] to match the ceramic substrates and semiconductors (like Al$_2$O$_3$, AlN, Si and GaAs). Finally, they should possess some other properties such as low densities, good mechanical performance and low costs[6].

Conventional metallic electronic packaging materials such as Cu, Al[7] Invar[8], Kovar[9] and super Invar[6], have been widely used. However, these materials are still have some negative attributes[9, 10]. To be specific, Cu and Al have high TC but their CTE are about four and five times larger than those of the semiconductor Si. It can induce high thermal stress in the electronic devices. Since the volume of magnetostriction counteracts the amount of thermal expansion at room temperature[11, 12], Invar and near-Invar alloys show very low, zero, or even negative in CTE, but their TC are low unfortunately[9, 13].

It is easy to consider that the Cu/Invar composites are good choice to meet new packaging materials requirements. There are many ways to prepare the Cu/Invar composites, such as multi-layer laminating, extruding, powder metallurgy and casting[10, 14-17]. Cu/Mo/Cu and Cu/Invar/Cu[4, 10, 18] are kinds of composites prepared by rolling or casting. Its middle layer is Invar alloy or Mo plate and both sides were covered with pure Cu. These materials combine high TC of Cu with low CTE of Invar alloy. However, these composites still have the shortcomings of material anisotropy and low interfacial bonding strength, which limited its application. Wu et al.[15] prepared Cu/Invar composites by power metallurgy. Stolk et al.[19] made

a nanocrystalline Cu/Invar composite by a novel solution-based synthesis technique and later sinter method. However, the Cu/Invar interface interdiffusion and holes in sintered samples are caused by the nearly no solid solubility of Fe, Co and Cu, which have adverse effects on the TC and CTE properties of Cu/Invar alloys.

Based on the calculation of phase diagrams (CALPHAD) method[20] and vacuum arc melting[17], several Cu-Fe$_{64}$Ni$_{32}$Co$_4$ alloys with different Cu contents were designed and synthesized. The Cu-Fe$_{64}$Ni$_{32}$Co$_4$ isotropic alloys present two separate fcc phases (fcc Cu-rich phase and fcc (Fe, Ni, Co)-rich phase) microstructures. In this study, the effects of annealing process and Cu contents on microstructures and thermophysical properties of the prepared alloys were investigated and discussed.

1 Experimental

1.1 Alloy design

Calculation phase diagrams method[20], as an effective tool of multi-component alloy design, is widely used in the design and development of new materials[17, 21-24]. For example, it can predict miscibility gaps, calculate liquids curves, vertical section diagram and the volume fraction of two liquid phases. Based on the thermodynamics database of the Cu-based alloys constructed by our group[25, 26], the Cu-Fe-Ni-Co quaternary phase diagram was calculated as shown in Fig.1. A large two fcc phases (fcc-(Cu) plus fcc-(Fe, Ni, Co)) equilibrium region constituted the main feature in the system. It is noteworthy that the solid solubility of two fcc phases decreases with the decreasing temperature, which may be useful for further an three alloys of Cu$_x$(Fe$_{0.64}$Ni$_{0.32}$Co$_{0.04}$)$_{100-x}$ (x=30, 45, 60, wt%)
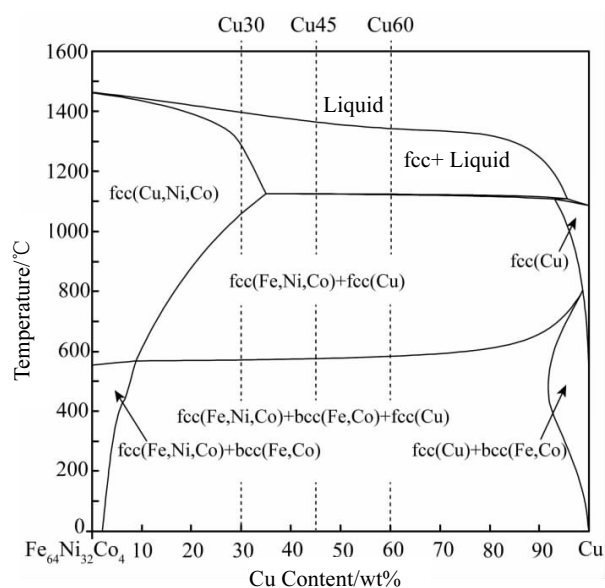

Fig.1 Calculated vertical section phase diagram of Cu-Fe$_{64}$-Ni$_{32}$Co$_4$[25, 26]

nealing process. Using the two fcc phases equilibrium region, were thus designed and named as alloys Cu30, Cu45 and Cu60, respectively. In this study, all mentioned chemical compositions are given in the form of mass ratio (wt%).

1.2 Materials and heat-treatments

As raw materials, high purity electrolytic copper (99.9 wt%), iron (99.7 wt%), nickel (99.9 wt%) and cobalt (99.9 wt%) were used. Three casting-ingots of Cu30 Cu45, and Cu60 alloys were prepared from above pure metals by arc-melting. In order to ensure compositional homogeneity, each button about 30 g was remelted at least five times. To eliminate the composition segregation and internal stress of the ingots, homogenization treatment at 1000 °C for 24 h followed by ice-water quenching was carried out. Subsequently, samples cut from ingots were annealed at 600 and 800 °C for various durations, and then quenched into ice-water.

1.3 Microstructures and crystal structure

Microstructural observation and composition measurement of each phase were carried out by electron probe microanalyzer (EPMA, JXA-8100, JEOL, Japan) with a 20 kV accelerating voltage and 1.0×10^{-8} A probe current. Crystal structure analysis was identified by Panalytical X'pert PRO X-ray diffractometer using Cu Kα radiation with a 40 kV voltage and 40 mA current. The data were collected in the range of 2θ from 20° to 100° at a step size of 0.0167°.

1.4 Thermophysical properties

All studied specimens for TC and CTE properties testing were cut by a wire-cutting machine. The sample size for CTE testing is 3 mm in diameter and 5 mm in height while that for TC testing is 12.7 mm in diameter and 2 mm in thickness.

CTE were measured by thermal mechanical analysis (TMA) and the average linear expansion coefficient α is calculated as follows[17]:

$$\alpha = \frac{1}{L_0} \frac{\Delta L}{\Delta t} \quad (1)$$

Where L_0, ΔL and Δt are the original length of the sample at room temperature, absolute length variation of specimen with the change of temperatures and test temperature range, respectively. The testing temperature ranges from 30 °C to 300 °C at a heating rate of 5 °C·min^{-1}. Archimedes method was employed to measure the density of the samples. TC was tested using LFA447 laser thermal conductivity analyzer and the TC (λ) was calculated as follows[14]:

$$\lambda = \alpha \rho C_p \quad (2)$$

where α, ρ and C_P are the thermal diffusion coefficient, density, specific heat capacity at constant pressure, respectively.

2 Results and Discussion

2.1 Microstructures and thermophysical properties of Cu30 alloy

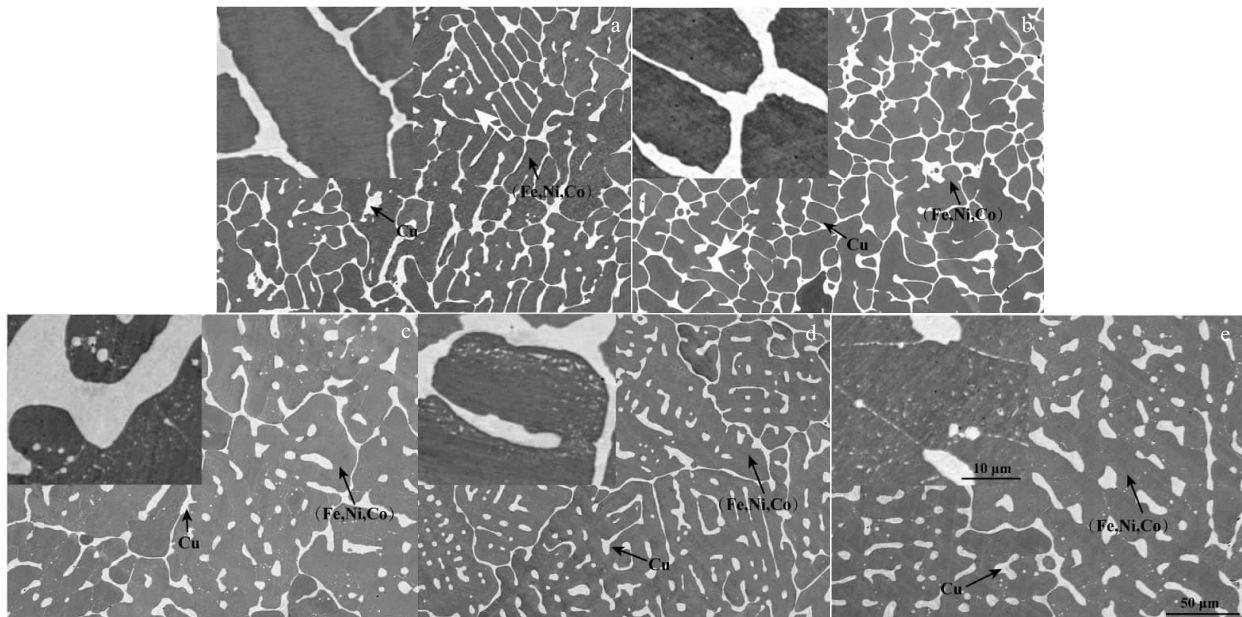Fig.2a shows the microstructures of Cu30 alloy quenched at

Fig.2   Microstructures of Cu30 alloy quenched at 1000 °C (a) and then annealed at 600 °C for different time: (b) 2 h, (c) 10 h, (d) 50 h, and
        (e) 100 h

1000 °C. Fig.2b~2e and Fig.3a~3d depict the microstructures of the Cu30 alloy with different annealing time at 600 and 800 °C, respectively. The white phase is referred as Cu-rich phase and the black matrix one belongs to (Fe, Ni, Co)-rich phase. Microstructures observations (Fig.2 and Fig.3) are consistent with the thermodynamic calculation result (Fig.1). From the Fig.2e and Fig.3d, it can be seen that Cu-rich phase grows and becomes coarse gradually at the grain boundary with the increase of annealing time.

Phase composition of Cu30 alloy annealed at 600 and 800 °C for different time are summarized in Table 1. From Table 1, it is found that the mass ratio of Fe, Ni and Co is approximately (65.68:30.16:4.16~65.97:29.82:4.21) in the (Fe, Ni, Co)-rich phase, which are close to Fe, Ni and Co mass percentage of 64:32:4 in super-Invar alloy.

In this study, in order to determine the phase structure of Cu30 alloy, the X-ray diffraction analysis of the quenched and annealed samples at different temperatures were tested, as shown in Fig.4. XRD results suggest that there are only fcc-(Cu) and fcc-(Fe, Ni, Co) diffraction peaks of Cu30 alloy. The positions of diffraction peaks of 600 °C annealed samples have no obvious changed compared with those annealed at 800 °C. Due to the extremely small difference in lattice parameter between fcc-Cu and fcc-(Fe, Ni, Co), all corresponding diffraction peaks are basically overlapped, as shown in Fig.4a. The results of XRD analysis further proves that Cu30 alloy presents two fcc phases microstructures.

Fig.5a~5b plots the annealing-time independently for CTE

and TC of the Cu30 alloy at 600 and 800 °C, respectively. All related CTE and TC data are given in Table 2. From the figures above, it implies that both CTE and TC values of the samples annealed at 600 °C are better than those of annealed at 800 °C. With the increase of annealing time from 2 to 50 h, the CTE curves show a decreasing trend and TC curves show an increasing trend. However, after annealing for 50 h, the changes of TC and CTE are not obvious.

As is known to all, the CTE of Cu is very high (about 17×10^{-6} K^{-1})[4], so the CTE of Cu-$Fe_{64}Ni_{32}Co_4$ is mainly decided by the (Fe, Ni, Co)-rich phase. However, the CTE is very sensitive to the composition in Invar alloy systems[16], which means that the purer the (Fe, Ni, Co)-rich phase, the lower the CTE in Cu-$Fe_{64}Ni_{32}Co_4$ alloys is. With the increase of annealing time, Cu atoms in the (Fe, Ni, Co)-rich phase are separated out constantly, thus causing a quick decreasing trend in CTE. Similarly, the much slower trend after 50 h in CTE should be attributed to the upcoming phase equilibrium state, which implies the finish of separating Cu process.

The TC of super-Invar alloy is very poor, about 13 $W \cdot (m \cdot K)^{-1}$[15, 27]. It is easy to understand that the TC of Cu-$Fe_{64}Ni_{32}Co_4$ alloys strongly depends on Cu content, which is accomplished by the movement of electrons[28]. When Cu content is very low (like Cu30 alloy in our case), it is hard to form a continuous net structure as an unobstructed thermal conduction channel, resulting in a low TC. Similar to the case of CTE transition, the Cu-rich phase precipitates from matrix and then grows and becomes coarse gradually at the grain
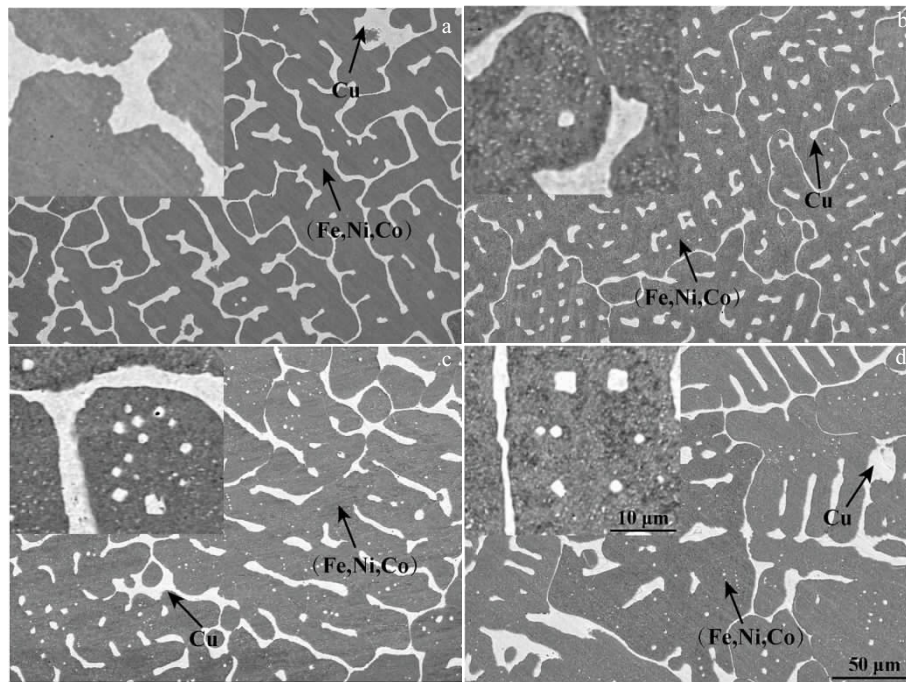
Fig.3   Microstructures of Cu30 alloy quenched at 1000 °C and then annealed at 800 °C for different time: (a) 2 h, (b) 10 h, (c) 50 h, and (d) 100 h

Table 1   Phase composition of Cu30 alloy annealed at 600 and 800 °C for different time in the range from 2 and 100 h

T/°C	t/h	(Fe, Ni, Co)-rich phase, content/wt%				Cu-rich phase, content/wt%			
		Cu	Fe	Ni	Co	Cu	Fe	Ni	Co
600	2	18.69	53.58	24.24	3.49	81.63	9.39	8.38	0.60
	10	18.62	53.61	24.32	3.45	82.04	9.14	8.23	0.59
	50	18.62	53.60	24.43	3.35	82.20	8.95	8.26	0.59
	100	18.59	53.62	24.44	3.35	82.21	9.01	8.18	0.60
800	2	19.24	53.04	24.36	3.36	81.81	9.31	8.26	0.62
	10	19.21	53.11	24.26	3.42	82.15	9.04	8.19	0.62
	50	19.06	53.28	24.27	3.39	82.33	8.95	8.11	0.61
	100	18.96	53.46	24.17	3.41	82.59	8.83	8.01	0.57

boundary with the increase of annealing time (Fig.2 and Fig.3). Besides, the (Fe, Ni, Co)-rich phase precipitates from Cu-rich phase, increasing the purity of Cu-rich phase. These two aspects promote the electron movement, resulting in a quick ascend in TC. Based on the above discussion, 50 h is considered to be the best time of heat treatment.

2.2   Microstructures and thermophysical properties of Cu45 and Cu60 alloys

The optimized parameter was adopted in Cu45 and Cu60 alloys for further study of the effects of Cu content on thermophysical properties. Fig.6a~6c and Fig.7a~7c depict the microstructures of Cu45 and Cu60 alloys quenched at 1000 °C and then annealed at 600 and 800 °C for 50 h, respectively.

Fig.6a~6c suggests that the black phase ((Fe, Ni, Co)-rich) is the matrix, whereas in Fig.7a~7c, the white phase (Cu-rich) becomes the matrix. Fig.8 shows the XRD patterns of the Cu45 and Cu60 alloys quenched at 1000 °C and annealed at 600 °C for 50 h. It indicates that there are only fcc-(Cu) and fcc-(Fe, Ni, Co) diffraction peaks of Cu45 and Cu60 alloys. The fcc-(Cu) and fcc-(Fe, Ni, Co) diffraction peaks of Cu45 and Cu60 alloys are basically overlapped as shown in Fig.8a, which are the same as the Cu30 alloy. The results of XRD analysis further prove that Cu45 and Cu60 alloys also show two fcc phases microstructures.

Fig.9 depicts the TC and CTE variation with an increasing Cu contents in Cu-Fe$_{64}$Ni$_{32}$Co$_4$ alloys at the formerly optimized
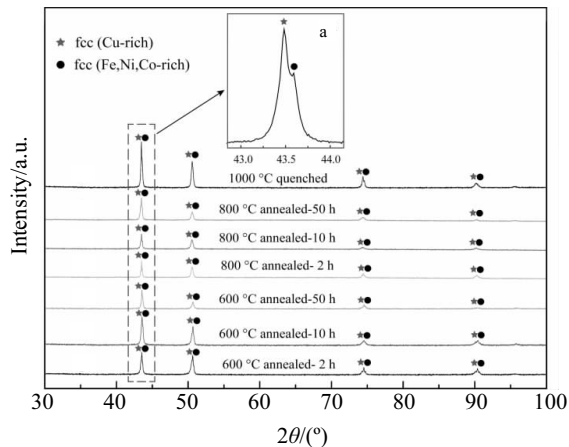
Fig.4   XRD patterns of the Cu30 alloy quenched at 1000 °C and then annealed at 600 and 800 °C for different time in the range from 2 h to 50 h
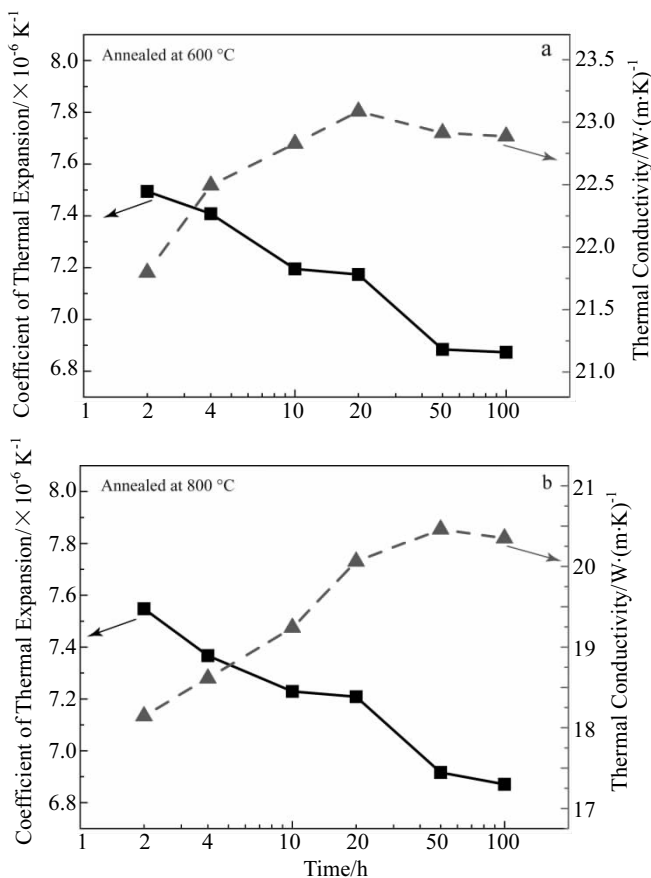

Fig.5   CTE and TC curves of Cu30 alloy annealed at 600 °C (a) and 800 °C (b) for different time in the range from 2 to 100 h

annealing-process (600 °C/800 °C for 50 h). All related TC and CTE data are summarized in Table 3 and Table 4, respectively. From Fig.9, it can be seen obviously that both TC and CTE have the similarl increasing trend. The TC of the samples an-

nealed at 600 °C are much greater than those of samples annealed at 800 °C. Compared with the TC of the samples, the CTE values of the samples annealed at different temperatures are close to each other. The higher temperature improves the solubility of Cu atoms in (Fe, Ni, Co)-rich phase (Fig.1 and Table 1), which increase the free electron scattering and decrease the Cu content, and this two aspects impedes the movement of electrons. Therefore, the TC of the samples annealed at 600 °C is higher than those of samples annealed at 800 °C. At the same time, the higher solubility of Cu atoms in (Fe, Ni, Co)-rich phase, reduces the purity of (Fe, Ni, Co)-rich phase, so the CTE of the samples annealed at 600 °C are better than those annealed at 800 °C. In general, annealing at low temperature is beneficial to the thermophysical properties of the alloys.

The TC of Cu45 and Cu60 alloys annealed at 600 °C for 50 h are 41.53 and 56.13 W·(m·K)$^{-1}$, respectively, which can be used as heat sink materials. However, the TC of Cu30 alloy is only 22.91 W·(m·K)$^{-1}$, which might be attributable to the low Cu contents. From Fig.6 and Fig.7, it is found that when the Cu contents increases up to 45 wt% and 60 wt%, the Cu-rich phase of the alloys forms a continuous net structure gradually. The continuous Cu net structure provides a transfer channel for electrons, so the TC of the alloys are significantly improved. When the Cu content is 30 wt% (Fig.2 and Fig.3), the (Fe, Ni, Co)-rich component is continuous, and the Cu-rich phase isolates in the (Fe, Ni, Co)-rich matrix, so the TC of Cu30 alloy is lower than that of Cu45 and Cu60 alloys. The CTE of Cu30 and Cu45 alloys after annealing at 600 °C for 50 h are 6.88×10^{-6} and 8.72×10^{-6} K^{-1}, respectively, which may match with semiconductor materials in electronic packaging. However, the CTE of Cu60 alloy is up to 12.36×10^{-6} K^{-1}, which may be due to that Invar effect is gradually weakened with the increase of Cu content in Cu-Fe$_{64}$Ni$_{32}$Co$_4$ alloys.

2.3 Calculation and prediction of CTE in Cu-Fe$_{64}$Ni$_{32}$Co$_4$ alloys

There are two models commonly used for the prediction of CTE in two-phase alloys, which are rule of mixtures (ROM) and Turner formula[29]. The ROM gives the thermal expansion α of a composite as follows:

$$\alpha = \alpha_1 V_1 + \alpha_2 V_2 \tag{3}$$

The Turner formula gives the thermal expansion α of a composite as follows:

$$\alpha = \frac{\alpha_1 V_1 E_1 + \alpha_2 V_2 E_2}{V_1 E_1 + V_2 E_2} \tag{4}$$

where α_1 and α_2, V_1 and V_2, E_1 and E_2 are the thermal expansion coefficients (17×10^{-6} K^{-1} for Cu and 0.5×10^{-6} K^{-1} for super-Invar), volume fractions, and elastic modulus (110 GPa for Cu and 145 GPa for super-Invar) of phases 1 and 2 in a composite, respectively.

The experimental CTE values and those calculation and predicted are given in Table 4. It indicates that CTE values decrease with the increase of (Fe, Ni, Co)-rich contents, and the

Table 2   Measured values of CTE and TC in Cu30 alloy annealed at different temperatures for different time

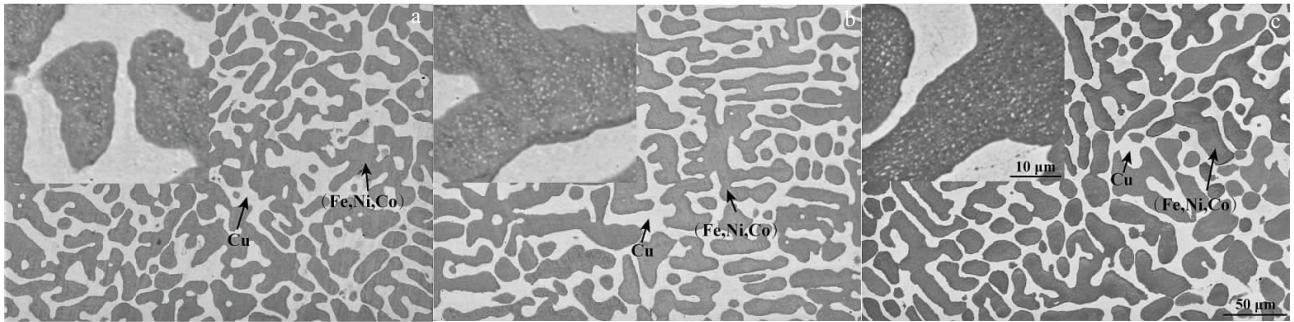| Thermophysical properties	Temperature/°C	Annealing time/h					
		2	4	10	20	50	100
CTE/×10⁻⁶ K⁻¹	600	7.49	7.41	7.20	7.17	6.88	6.87
	800	7.55	7.37	7.22	7.21	6.91	6.87
TC/W·(m·K)⁻¹	600	21.80	22.49	22.83	23.09	22.91	22.89
	800	18.14	18.61	19.24	20.16	20.46	20.35

Fig.6   Microstructures of Cu45 alloys quenched at 1000 °C (a) and then annealed at 600 (b) and 800 °C (c) for 50 h
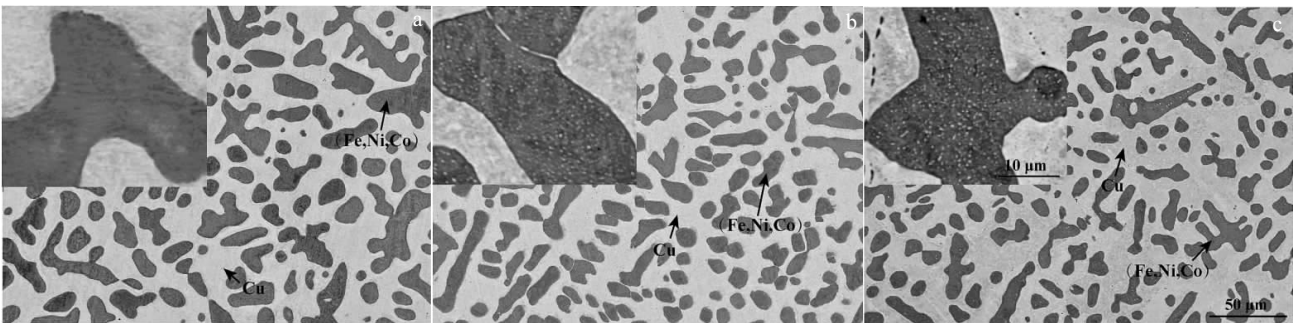

Fig.7   Microstructures of Cu60 alloys quenched at 1000 °C (a) and then annealed at 600 (b) and 800 °C (c) for 50 h
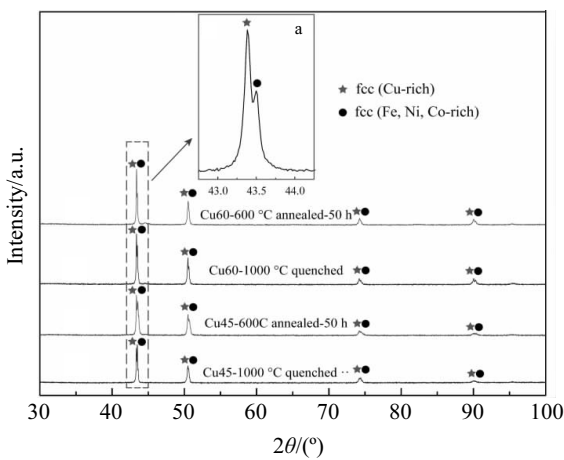

Fig.8   XRD patterns of the Cu45 and Cu60 alloys quenched at 1000 °C and then annealed at 600 °C for 50 h
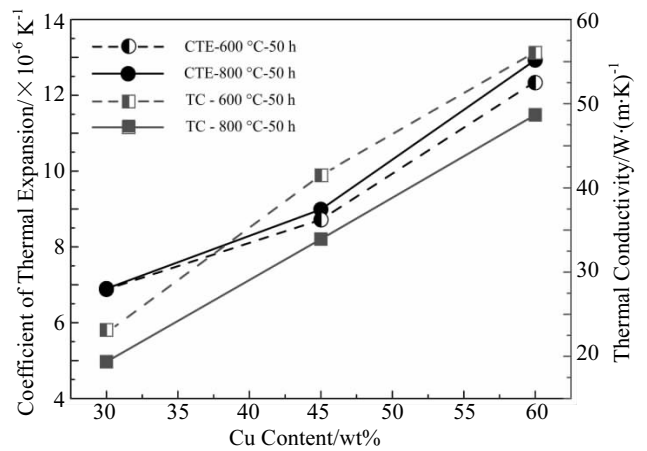
Fig.9   CTE and TC curves of $Cu_x(Fe_{0.64}Ni_{0.36}Co_{0.04})_{100-x}$ (x=30, 45, 60 wt%) alloys annealed at 600 and 800 °C for 50 h

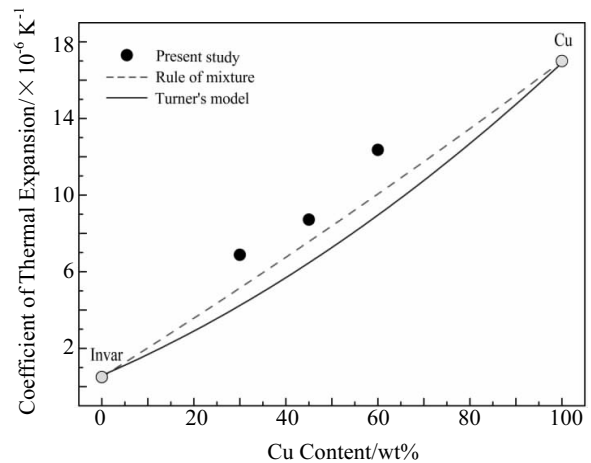**Table 3   TC of Cu$_x$(Fe$_{0.64}$Ni$_{0.32}$Co$_{0.04}$)$_{100-x}$(x=30, 45, 60, wt%) alloys with different heat treatment processes [W·(m·K)$^{-1}$]**

Sample	Cast	1000 °C quenched	800 °C annealed for 50 h	600 °C annealed for 50 h
Cu30	18.52	18.23	20.46	22.91
Cu45	25.67	24.41	33.92	41.53
Cu60	47.32	43.35	48.67	56.13

alloys annealed at 600 °C for 50 h have the smallest CTE values. CTE of the quenched specimens are slightly higher than those of the ingots, which may be related to the internal stress within the quenched specimens.

Fig.10 shows the CTE of the present Cu30, Cu45 and Cu60 alloys annealed at 600 °C for 50 h and those CTE fitting curves by calculation and prediction. It suggests that, those fitting curves are deviated from the actually measured values. Compared with Turner's model, average CTE values of the present composites are close to the values predicted by ROM. Two reasons may account for the experimental CTE values higher than those predicted by Turner's model. On the one hand, Invar effect are very sensitive to the composition of the alloy, only when the mass percentage of Fe:Ni:Co is infinitely close to 64:32:4, can super-Invar alloy maintain very low CTE values[19]. However, from Fig.1, it can be found that there is a certain amounts of solid solubility of Cu in (Fe, Ni, Co)-rich phase or Fe, Ni and Co in Cu-rich phase. Besides, deviations of the Fe, Ni and Co ratios from above values, results in a significant in-

crease in the CTE of the alloys. On the other hand, Turner's model assumes that there is only equilibrium of internal stress existing between the Cu-rich phase and (Fe, Ni, Co)-rich phase[28,30]. However, in the process of preparing Cu-Fe$_{64}$Ni$_{32}$Co$_4$ alloys, the complex internal stress will be produced when alloys are cooled from high temperatures, and the calculation and prediction CTE results are often much smaller than the experiment CTE values.

Fig.10   CTE curves of the present Cu$_x$(Fe$_{0.64}$Ni$_{0.32}$Co$_{0.04}$)$_{100-x}$(x=30, 45, 60, wt%) composites annealed at 600 °C for 50 h compared with those CTE fitting curves by calculation and prediction

Table 4   Experimental CTE of the calculated and predicted of Cu$_x$(Fe$_{0.64}$Ni$_{0.32}$Co$_{0.04}$)$_{100-x}$(x=30, 45, 60, wt%) alloys ($\times 10^{-6}$ K^{-1})

Sample	Cast	1000 °C quenched	800 °C annealed for 50 h	600 °C annealed for 50 h	ROM model	Turner's model
Cu30	7.65	7.68	6.91	6.88	5.15	4.29
Cu45	9.60	10.29	8.99	8.72	7.57	6.48
Cu60	14.04	14.15	12.93	12.36	10.05	8.93

3   Conclusions

1) All the prepared Cu-Fe$_{64}$Ni$_{32}$Co$_4$ alloys present two separate fcc phases (fcc Cu-rich phase and fcc (Fe, Ni, Co)-rich phase) microstructures.

2) The optimized annealing process, 600 °C for 50 h, is obtained from the studied Cu30 alloy, which has a CTE of 6.88×10^{-6} K^{-1} and a TC of 22.91 W·(m·K)$^{-1}$.

3) Among the three alloys, the Cu45 alloy at 600 °C annealed for 50 h has fine comprehensive properties with a CTE of 8.72×10^{-6} K^{-1} and a TC of 41.53 W·(m·K)$^{-1}$. It not only can be used for heat sink applications, but also match the CTE of the semiconductor material in electronic packaging.

References

1   Zweben C. *Journal of the Minerals, Metals & Materials Society*[J], 1998, 50(6): 47

2   Shen Y L, Needleman A, Suresh S. *Metallurgical & Materials Transactions A*[J], 1994, 25(4): 839

3   Zweben C. *Proceedings of International Symposium on Advanced Packaging Materials: Processes, Properties and Interfaces*[C]. Braselton: IEEE, 2002

4   Yang H J Wang Z F, Wang H S *et al. Materials Review*[J], 2004, 18(6): 86 (in Chinese)

5   Ryelandt S, Mertens A, Delannay F. *Materials & Design*[J], 2015, 85: 318

6   Zhang Y J, Wang Z F, Lv W J *et al. Materials Review*[J], 1997, 11(3): 52 (in Chinese)

7   Yu X B, Wu R J, Zhang G D. *Materials Review*[J], 1994, (3): 64 (in Chinese)

8   Li Q L, Hu D C. *Mechanical Management and Development*[J], 2007, 48(7): 1815 (in Chinese)

9   Tong Z S, Sheng Z S. *Electronics & Packaging*[J], 2005, 5(3): 6 (in Chinese)

10　Cai H, Wang Y P, Song X P *et al. Materials Review*[J], 2009, 23(15): 24 (in Chinese)

11　Shiga M. *Current Opinion in Solid State & Materials Science*[J], 1996, 1(3): 340

12　Moriya T, Kan U. *Solid State Communications*[J], 1980, 34(2): 95

13　Xing S M. *Spacecraft Recovery & Remote Sensing*[J], 1998, (3): 37 (in Chinese)

14　Jha S. *Proceedings of Electronic Components and Technology Conference*[C]. Las Vegas, Nevada: IEEE, 1995

15　Wu D, Wu S P, Yang L *et al. Powder Metallurgy*[J], 2014, 58(2): 1743290114Y.000

16　Cottle R D, Chen X, Jain R K *et al. Journal of the Minerals, Metals & Materials Society*[J], 1998, 50(6): 67

17　Liu X J, He Z F, Shi Z *et al. Journal of Xiamen University*[J], 2014, 53(4): 538 (in Chinese)

18　Cheng T Y, Xiong N, Cheng W U *et al. Materials for Mechanical Engineering*[J], 2010, 34(3): 38 (in Chinese)

19　Stolk J, Manthiram A. *Materials Science & Engineering B*[J], 1999, 60(2): 112

20　Sundman Bo, Jansson Bo, Andersson J O. *Calphad-computer Coupling of Phase Diagrams & Thermochemistry*[J], 1985, 9(2): 153

21　Wang C P, Liu X J, Kainuma R *et al. Metallurgical & Materials Transactions A*[J], 2004, 35(4): 1243

22　Wang C P, Liu X J, Ohnuma I *et al. Science*[J], 2002, 297(5583): 990

23　Yu Y, Takaku Y, Nagasako M *et al. Intermetallics*[J], 2012, 25: 95

24　Wang C P, Liu X J, Ohnuma I *et al. Journal of Materials Research*[J], 2008, 23(4): 933

25　Wang C P, Liu X J, Jiang M *et al. Journal of Physics & Chemistry of Solids*[J], 2005, 66(2-4): 256

26　Liu X J, Wang C P, Gan S X *et al. Chinese Journal of Nonferrous Metals*[J], 2011, 21(10): 2511 (in Chinese)

27　Zweben C. *Proceedings of SPI-the International Society for Optical Engineering*[C]. San Jose: SPIE, 2008

28　Jing Z, Peng C Q, Wang R C *et al. Chinese Journal of Nonferrous Metals*[J], 2015, 25(12): 3255 (in Chinese)

29　Fahmy A A, Ragai A N. *Journal of Applied Physics*[J], 1970, 41(13): 5108

30　Lee J I, Park E S. *Journal of Materials Research*[J], 2016, 32(1): 217

Cu-Fe$_{64}$Ni$_{32}$Co$_4$合金显微组织及热物理性能

王翠萍[1]，乐帆程[1]，朱家华[1]，杨木金[1]，杨水源[1]，张锦彬[1]，石田清仁[3]，刘兴军[1, 2]

(1. 厦门大学 福建省材料基因工程重点实验室，福建 厦门 361005)

(2. 哈尔滨工业大学(深圳)，广东 深圳 518055)

(3. 东北大学大学院工学研究科，仙台 980-8579，日本)

摘　要：利用相图计算的 CALPHAD 方法和真空电弧熔炼技术，设计并制备了 Cu$_x$(Fe$_{0.64}$Ni$_{0.32}$Co$_{0.04}$)$_{100-x}$(x=30, 45, 60, 质量分数, %)系列合金。实验研究了该系列合金在不同热处理工艺时的显微组织，热导率以及热膨胀系数。结果表明：Cu-Fe$_{64}$Ni$_{32}$Co$_4$ 系列合金在 600 和 800 ℃时效处理后均为 fcc 富铜相和 fcc 富因瓦 (铁镍钴) 相组成的各向同性的多晶合金。该系列合金在 1000 ℃淬火并在 600 ℃时效处理 50 h 后，其热膨胀系数变化范围为 6.88×10^{-6}~12.36×10^{-6} K^{-1}；热导率变化范围为 22.91~56.13 W·(m·K)$^{-1}$；其热导率明显高于因瓦合金，其中 Cu$_{30}$(Fe$_{0.64}$Ni$_{0.32}$Co$_{0.04}$)$_{70}$ 与 Cu$_{45}$(Fe$_{0.64}$Ni$_{0.32}$Co$_{0.04}$)$_{55}$ 合金的热膨胀系数可以与电子封装中半导体材料的热膨胀系数相匹配。

关键词：CALPHAD方法；Cu-Fe$_{64}$Ni$_{32}$Co$_4$合金；显微组织；热导率；热膨胀系数

作者简介：王翠萍，女，1965 年生，博士，教授，厦门大学材料学院，福建 厦门 361005，电话：0592-2187888，E-mail: wangcp@xmu.edu.cn